

Transformer Current Ringing in Dual Active Bridge Converters

Qin, Z.; Shen, Zhan; Blaabjerg, Frede; Bauer, P.

DOI

[10.1109/TIE.2020.3040681](https://doi.org/10.1109/TIE.2020.3040681)

Publication date

2020

Document Version

Final published version

Published in

IEEE Transactions on Industrial Electronics

Citation (APA)

Qin, Z., Shen, Z., Blaabjerg, F., & Bauer, P. (2020). Transformer Current Ringing in Dual Active Bridge Converters. *IEEE Transactions on Industrial Electronics*, 68(12), 12130-12140. Article 9280428. <https://doi.org/10.1109/TIE.2020.3040681>

Important note

To cite this publication, please use the final published version (if applicable). Please check the document version above.

Copyright

Other than for strictly personal use, it is not permitted to download, forward or distribute the text or part of it, without the consent of the author(s) and/or copyright holder(s), unless the work is under an open content license such as Creative Commons.

Takedown policy

Please contact us and provide details if you believe this document breaches copyrights. We will remove access to the work immediately and investigate your claim.

Transformer Current Ringing in Dual Active Bridge Converters

Zian Qin , Senior Member, IEEE, Zhan Shen , Member, IEEE, Frede Blaabjerg , Fellow, IEEE, and Pavol Bauer , Senior Member, IEEE

Abstract—In dual active bridge (DAB) converters, there can be transformer current ringing, especially when the transformer turns ratio is high. It is induced by high dv/dt generated by fast switching as well as the low impedance of the magnetic tank at the high-frequency range. To quantify the influence of the magnetic tank, its impedance model is thoroughly modeled by considering all the parasitic components. It is found that the parasitic capacitors of the magnetics do not equally affect the current ringing, and thereby the critical one is addressed. On top of that, the design guide of the inductor is provided for the mitigation of the current ringing. Additionally, the impact of dv/dt is also studied. The models and analyses are verified on a 2.5-kW DAB prototype.

Index Terms—Current ringing, dual active bridge (DAB) converter, dv/dt , impedance model, magnetic tank.

I. INTRODUCTION

THE dual active bridge (DAB) converter [1], due to its simple topology and control, galvanic isolation, bidirectional power flow, wide input and output voltage adaptive range, high power density, and efficiency, is very promising in applications, such as solid-state transformers (SSTs) [2]–[4], electric vehicle chargers with V2G concept [5], [6], and power flow control in dc grids [7]–[9].

DAB is known as a converter with soft switching but when the load is very light or the input/output voltage deviates a lot from the rated value, it can hardly maintain soft switching. Then not only the power loss is increased but also electromagnetic interference (EMI) issues get worse. Various modulation strategies were, therefore, proposed to extend the soft-switching region [10]–[12].

Wide bandgap device-based DABs were studied in the literature not only for higher efficiency but mainly for either a higher voltage rating, such as SiC-based DAB in SSTs [2] or a more

compact design, such as GaN-based DAB in an onboard charger [5]. In both scenarios, dv/dt is pushed to very high. Then EMI issues become more critical [13], [14]. The reason is that the magnetic tank of the DAB, as shown in Fig. 1, has a parasitic capacitance, which changes the impedance of the magnetic tank from inductive to capacitive at a high frequency, where the impedance has a shallow magnitude. Together with a high dv/dt , the current ringing and thereby EMI become significant. The current ringing may also lead to more power loss in the converter since the ac resistance of the wire at the ringing frequency is much higher than the fundamental frequency [15].

The current ringing issues can be eliminated by adding a parallel capacitance to the switches to reduce dv/dt [13], where the full parasitic model of the transformer is also considered in the impedance modeling. However, the turn-ON switching loss will increase when the converter enters into hard switching, and a larger capacitor in parallel also makes the soft switching more challenging to achieve since more energy is needed to discharge the capacitor. Moreover, lower dv/dt limits the switching frequency in terms of duty ratio loss. Finally, in practice, one or two series inductors are needed in the magnetic tank for the power flow control, which contributes considerable stray capacitance and should also be considered [15].

Another promising method to decrease the current ringing is to improve the impedance of the magnetic tank. Therefore, the detailed modeling of the parasitics of the magnetic tank, i.e., stray capacitance, leakage inductance, and ac resistance, is essential. For the stray capacitance modeling, various structure-based analytical methods are reviewed in [16]. The impact of the various winding architectures and wire types is discussed in [17]–[24]. The stray capacitance of planar transformers is a severe issue, and the tradeoff between the stray capacitance, ac resistance, and leakage inductance is discussed in [25]–[27]. For the ac resistance of winding, Dowell [28] has proposed the classic formula, which considers both the skin and proximity effect in the high-frequency range. It assumes that the magnetic flux is straight and is modified and improved by considering the flux distortion [29], [30] and the phase shift of the current [31] in recent advances. The analytical model of the Litz wire winding resistance is proposed in [32]. The analytical leakage inductance models are also based on the physical structure of magnetics. Dowell also gives the one-dimensional expression of leakage inductance in [28]. It is later developed by considering the more detailed winding and core structure into the analysis [35]. Furthermore, the leakage inductance of magnetics

Manuscript received May 18, 2020; revised August 31, 2020 and October 20, 2020; accepted November 12, 2020. Date of publication December 3, 2020; date of current version August 25, 2021. (Corresponding author: Zhan Shen.)

Zian Qin and Pavol Bauer are with the Department of Electrical Sustainable Energy, DCE&S Group, Delft University of Technology, 2600 Delft, The Netherlands (e-mail: zqi@ieee.org; p.bauer@tudelft.nl).

Zhan Shen and Frede Blaabjerg are with the Department of Energy Technology, Aalborg University, 9220 Aalborg, Denmark (e-mail: zhs@et.aau.dk; fbl@et.aau.dk).

Color versions of one or more of the figures in this article are available at <https://doi.org/10.1109/TIE.2020.3040681>.

Digital Object Identifier 10.1109/TIE.2020.3040681

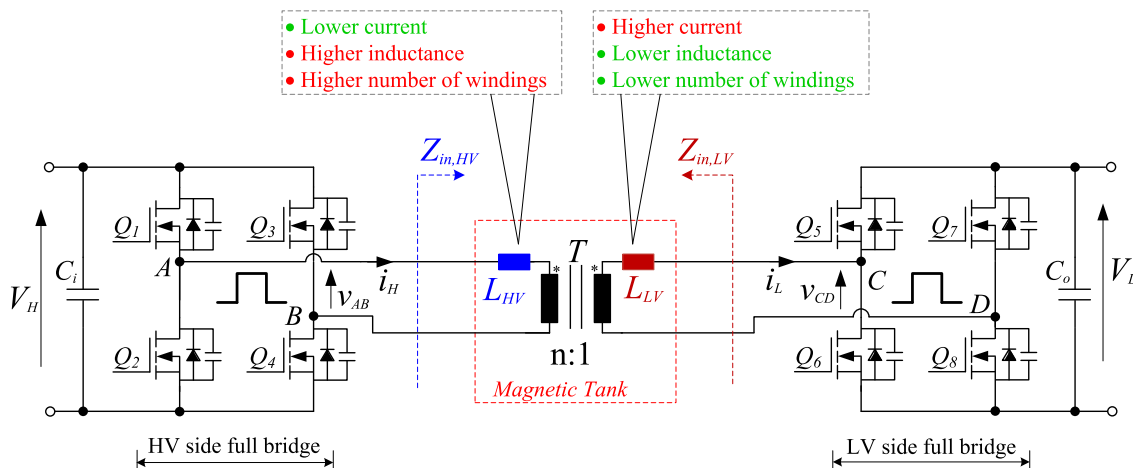


Fig. 1. DAB converter. To realize the large leakage inductance of the transformer T for power transforming, a standalone inductor is added to the HV side (L_{HV}), low-voltage side (L_{LV}), or both sides.

with the Litz wire [38], unparallel winding [39], nonidea winding [24], and different winding shapes and configurations [40]–[42] are investigated through the detailed magnetic field flux modeling, respectively. In general, those research works focus on the physical-structure-based parasitic modeling of single magnetic components. Their models can be used in the inductor–transformer-combined magnetic tank modeling in this study at the circuit level.

At the circuit level, Saket *et al.* [26], Zdanowski *et al.* [43], and Hernandez *et al.* [44] have verified that by decreasing the stray capacitance of magnetics, the current ringing as well as the measured EMI reduces dramatically. The research in [45] solves this issue by improving the layout of the planar transformer. The concept of the paired layer is proposed in [46] and it achieves a small dv/dt as well as a significant reduction of the common-mode (CM) noise in the flyback and forward converter. The transformer capacitance network of a flyback converter is also studied in [47] to reduce its CM noise. Furthermore, the Faraday shield is a powerful structure to minimize the transformer interwinding capacitance as well as the CM noise [47], [48]. Moreover, by precisely controlling the leakage inductance in the DAB [49] and *LLC* resonant converter [50], the circuit performance, control flexibility, and efficiency are improved. However, for those methods, a specific analysis and design of the transformer layer structure are needed. For the active solution of the current ringing mitigation, the research in [51] uses the active harmonic suppression strategy in the modulation to decrease the dc-bus harmonic of DAB.

Yet in those studies, only the impact of the sole parasitic of the single magnetic component is considered. A quantified model in the inductor–transformer-combined magnetic tank considering all parasitics, i.e., the stray capacitance, leakage inductance, and ac resistance, and their impacts on various high-frequency aspects, e.g., current ringing, EMI, and efficiency, is still rare.

Our previous conference work presents a simple model of the magnetic tank [52]. In this article, a more complete and concrete impedance modeling and analysis are presented, where the impact of the different parasitic capacitors in the magnetic

tank is quantified to address the critical one. Moreover, the leakage inductance and the equivalent resistance are also considered. Furthermore, the impact of dv/dt on the current ringing is also quantified and the experimental verification is enriched. The results can be used as a guide for the converter designer. The rest of the article is organized as follows. The impedance of the magnetic tank is modeled in Section II. Then based upon the model, the current ringing is analyzed in Section III, where the mitigation measure is also discussed and the design guide is provided. The work is then verified in Section IV and Section V concludes this article.

II. MAGNETIC TANK IMPEDANCE MODELING

As shown in Fig. 1, a DAB converter is composed of two full bridges and a magnetic tank. The former contains eight power switches $Q_1 \sim Q_8$ and two capacitors C_i and C_o . v_{AB} and v_{CD} are the two voltages generated by the high-voltage (HV) and LV-side full bridge, respectively. The magnetic tank includes a transformer T and an inductor. The standalone inductor is to add the leakage inductance of the transformer with a smaller power loss compared with a single transformer with considerable leakage. In the literature, the inductor has been connected to the HV winding, low-voltage winding, or both. There are pros and cons to connect the inductor differently, as summarized in Fig. 1, but how they can influence the transformer current ringing is unclear. Thus, to make the analysis more generic, it is assumed that the inductor is split into two, L_{HV} and L_{LV} for the high and low-voltage windings, respectively, and their equivalent inductances are identical. $Z_{in,HV}$ and $Z_{in,LV}$ are the input impedance of the magnetic tank at the high and low-voltage side, respectively. Then the current ringing on the HV side is influenced by the dv/dt on the HV side and $Z_{in,HV}$, while the current ringing on the LV side is influenced by the dv/dt on the LV side and $Z_{in,LV}$.

The generic impedance models of the transformer and inductor are used for analysis, and they are shown in Figs. 2

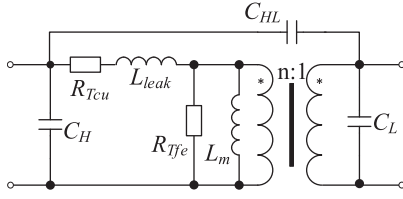
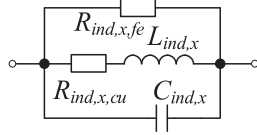


Fig. 2. Impedance model of a two-winding transformer.



Note: x can be H or L

Fig. 3. Impedance model of an inductor.

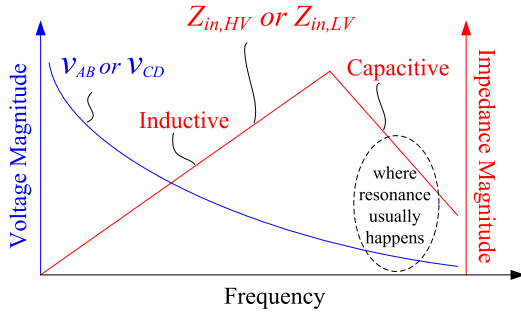


Fig. 4. Diagram to show the spectrum of the input voltage and impedance of the magnetic tank.

and 3. In the transformer model, L_m is the magnetizing inductance; L_{leak} is the leakage inductance; C_H and C_L are the HV- and LV-side winding capacitance; C_{HL} is the coupling capacitance between the two windings; R_{Tcu} is the winding resistance; R_{Tfe} is the equivalent resistance indicating the core loss. The inductor model is composed of an inductor $L_{ind,x}$, a capacitor $C_{ind,x}$ in parallel, a winding resistance $R_{ind,x,cu}$, and an equivalent resistance $R_{ind,x,fe}$ regarding the core loss. At a low frequency, the inductance dominates the impedance, while at a high frequency, the capacitance will take over. So both $Z_{in, HV}$ and $Z_{in, LV}$ will have an impedance curve, as depicted in Fig. 4. Depending on the modulation scheme (single-phase

shift, dual-phase shift, and triple-phase shift) used in the DAB, the input voltage of the magnetic tank v_{AB} and v_{CD} can be both square, one square and one three-level hybrid, or both three-level waveforms. Regardless, v_{AB} and v_{CD} will have a spectrum, as shown in Fig. 4. It can be seen that as the frequency increases the magnitude of voltage harmonics will decrease and the impedance will increase, which makes the current ringing hardly happen below the corner frequency but beyond that frequency, the impedance starts to decline and it largely boosts the chance of current ringing. To concretely analyze the current ringing, the two impedances of the magnetic tank are thoroughly modeled, as shown in Figs. 5 and 6. The modeling procedure is elaborated in the Appendix.

Assuming the inductor is only connected to either the HV or LV side, then from Figs. 5(d) and 6(d), the equations (1)–(4) at the bottom of this page and the following equations can be obtained:

$$R_A = \frac{n^2 R_{Tfe} R_{ind,L,fe}}{R_{Tfe} + n^2 R_{ind,L,fe}} \quad (5)$$

$$C_A = C_H + \frac{C_{ind,L} + C_L}{n^2} + (1 - 1/n)^2 C_{HL}/4 \quad (6)$$

$$R_B = \frac{R_{Tfe} R_{ind,H,fe}}{n^2 (R_{Tfe} + R_{ind,H,fe})} \quad (7)$$

$$C_B = n^2 (C_{ind,L} + C_H) + C_L + (n - 1)^2 C_{HL}/4 \quad (8)$$

where $Z_{in, HV} |_{L_{ind,L}=0}$ and $Z_{in, LV} |_{L_{ind,L}=0}$ depict the input impedance of the magnetic tank from the HV and LV side, respectively, and meanwhile, the inductor is connected only on the HV side; $Z_{in, HV} |_{L_{ind,H}=0}$ and $Z_{in, LV} |_{L_{ind,H}=0}$ depict the input impedance of the magnetic tank from the HV and LV side, respectively, and meanwhile, the inductor is connected only on the low-voltage side.

According to (1)–(4) shown at the bottom of this page, the impedance of the magnetic tank can always be modeled as the LC parallel resonant circuit in series with the leakage inductance if there is only one inductor. Another LC parallel resonant circuit will be added to the model if there are two inductors. To make it clearer, the impedance model of the magnetic tank is also summarized in Table I.

It should be noted that the developed model is intended for the high-frequency current ringing study. It guides the converter

$$Z_{in, HV} |_{L_{ind,L}=0} = \frac{R_{ind,H,fe} (sL_{ind,H} + R_{ind,H,cu})}{s^2 L_{ind,H} C_{ind,H} R_{ind,H,fe} + s (L_{ind,H} + C_{ind,H} R_{ind,H,fe} R_{ind,H,cu}) + R_{ind,H,fe} + R_{ind,H,cu}} + sL_{leak} + R_{Tcu} \quad (1)$$

$$Z_{in, HV} |_{L_{ind,H}=0} = \frac{R_A (sn^2 L_{ind,L} + n^2 R_{ind,L,cu})}{s^2 n^2 L_{ind,L} C_A R_A + sn^2 (L_{ind,H} + C_A R_A R_{ind,H,cu}) + R_A + n^2 R_{ind,H,cu}} + sL_{leak} + R_{Tcu} \quad (2)$$

$$Z_{in, LV} |_{L_{ind,L}=0} = \frac{R_B (sL_{ind,H} + R_{ind,H,cu})}{s^2 L_{ind,H} C_B R_B + s (L_{ind,H} + C_B R_B R_{ind,H,cu}) + n^2 R_B + R_{ind,H,cu}} + \frac{sL_{leak}}{n^2} + \frac{R_{Tcu}}{n^2} \quad (3)$$

$$Z_{in, LV} |_{L_{ind,H}=0} = \frac{R_{ind,L,fe} (sL_{ind,L} + R_{ind,L,cu})}{s^2 L_{ind,L} C_{ind,L} R_{ind,L,fe} + s (L_{ind,L} + C_{ind,L} R_{ind,L,fe} R_{ind,L,cu}) + R_{ind,L,fe} + R_{ind,L,cu}} + \frac{sL_{leak}}{n^2} + \frac{R_{Tcu}}{n^2} \quad (4)$$

TABLE I
IMPEDANCE MODEL OF THE MAGNETIC TANK

Condition	Impedance	Comment
$Z_{in,HV} _{L_{ind,L}=0}$ Only HV side inductor		Only $C_{ind,H}$ matters. Design challenge is low
$Z_{in,LV} _{L_{ind,L}=0}$		The impact of C_H , $C_{ind,H}$ and C_{HL} are much amplified Design challenge is high
$Z_{in,HV} _{L_{ind,H}=0}$ Only LV side inductor		Mainly the C_H and C_{HL} influence. Design challenge is medium
$Z_{in,LV} _{L_{ind,H}=0}$		Only $C_{ind,L}$ matters Design challenge is low

hardware designers since it clearly shows how the different parasitic capacitances influence the current ringing with varying factors of weight. The developed model is not for the power flow control or output-voltage control. The reason is that the parasitic capacitors have a minor impact on the power flow or output voltage, which are, therefore, ignored in modeling for the power flow control. However, the developed model is useful in the gate voltage control or dv/dt control, which controls the slew rate of the drain–source voltage during switching by controlling the gate voltage or gate resistance.

III. CURRENT RINGING ANALYSIS AND MITIGATION

A. Influence of the Magnetic Tank

As seen in Table I, if there is only one inductor in the magnetic tank, then to keep the equivalent inductance the same, it is required in the design of DAB that

$$L_{ind,H} = n^2 L_{ind,L}. \quad (9)$$

Therefore, the LV-side input impedance $Z_{in,LV}$ always has an inductance n^2 times smaller than the HV-side input impedance $Z_{in,HV}$. That is why, in general, the current ringing is often observed in the LV-side winding of the transformer rather than the HV side. However, the impact of the parasitic capacitance is not considered so far. Second, for $Z_{in,HV}$, if the inductor is connected to the HV side, the equivalent capacitance of the impedance is mainly the capacitance of the HV-side inductor. If the inductor is connected to the LV side, the equivalent capacitance of the impedance is dominated by the HV-side

winding capacitance and coupling capacitance of the transformer. Meanwhile, the impact of the LV-side winding capacitance and LV-side inductor capacitance is attenuated by n^2 times. For $Z_{in,LV}$, if the inductor is connected to the LV side, the equivalent capacitance of the impedance is mainly the capacitance of the LV-side inductor. If the inductor is connected to the HV side, the equivalent capacitance of the impedance is affected mostly by the HV-side inductor capacitance, the HV-side winding capacitance, and the coupling capacitance of the transformer.

B. Influence of dv/dt

Additionally, as discussed in Fig. 4, the current ringing is also influenced by the voltages v_{AB} and v_{CD} generated by both the HV and LV-side full bridges. To be more specific, it is the dv/dt of v_{AB} and v_{CD} that affects the current ringing. For a thorough analysis, the spectrums of two trapezoidal waveforms are obtained and they are shown in Fig. 7. Both of them have a 50% duty ratio and the same magnitude, and only dv/dt differs. According to [53], the spectrums both have two corner frequencies. The first one is $f_s/0.5\pi$. Since it is lower than switching frequency f_s , it is invisible in the spectrum. The second corner frequency is $1/(\pi\tau)$, where τ is the rising time of the waveform. The two trapezoidal waveforms both have a magnitude as ± 110 V. Thus, the second corner frequency can be calculated with given dv/dt and it is $f_1 = 1.45$ MHz and $f_2 = 2.89$ MHz. Below the second corner frequency, the envelope of the spectrum decreases at a rate of -20 dB per decade, while above the second corner

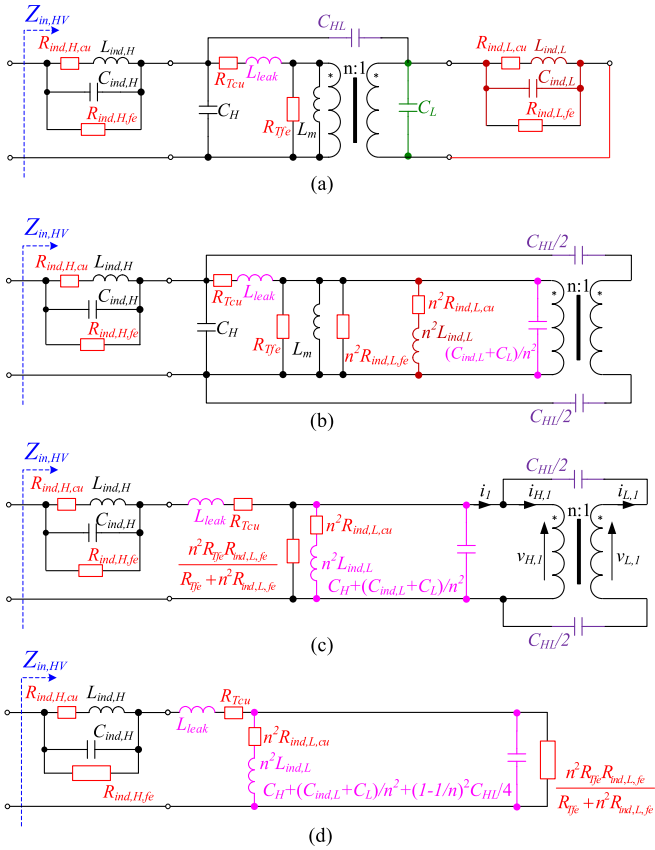


Fig. 5. HV-side input impedance model of the magnetic tank. (a) Detailed model. (b) Intermediate model 1. (c) Intermediate model 2. (d) Simplified model.

frequency, the envelope decreases at a rate of -40 dB per decade. Thus, it can be concluded that different dv/dt will lead to a different second corner frequency and different magnitude of the spectrum after the second corner frequency. Higher the dv/dt , higher the magnitude of the spectrum after the second corner frequency, and higher the chance of current ringing.

C. Current Ringing Mitigation

To mitigate the current ringing, one way is to increase the impedance of the magnetic tank at the frequency of interest; another is to slow down dv/dt . There are two typical approaches to slow down dv/dt , as follows:

- 1) using larger gate resistance;
- 2) adding more capacitance in parallel with the switches.

Both of the two approaches will increase the switching loss in case the converter operates in hard switching. As known, DAB will inevitably enter into hard-switching mode when the load is very low or the voltage deviates much from the optimal point. Even in the soft-switching mode, although the switching loss will not increase, the switching frequency will be limited due to the duty ratio loss. Therefore, for medium and high-frequency DAB, improving the magnetic tank is the better way to go for the transformer current ringing mitigation. And as analyzed above and commented in Table I, the most promising way is to add the inductor in the LV side of the transformer. Then the inductor

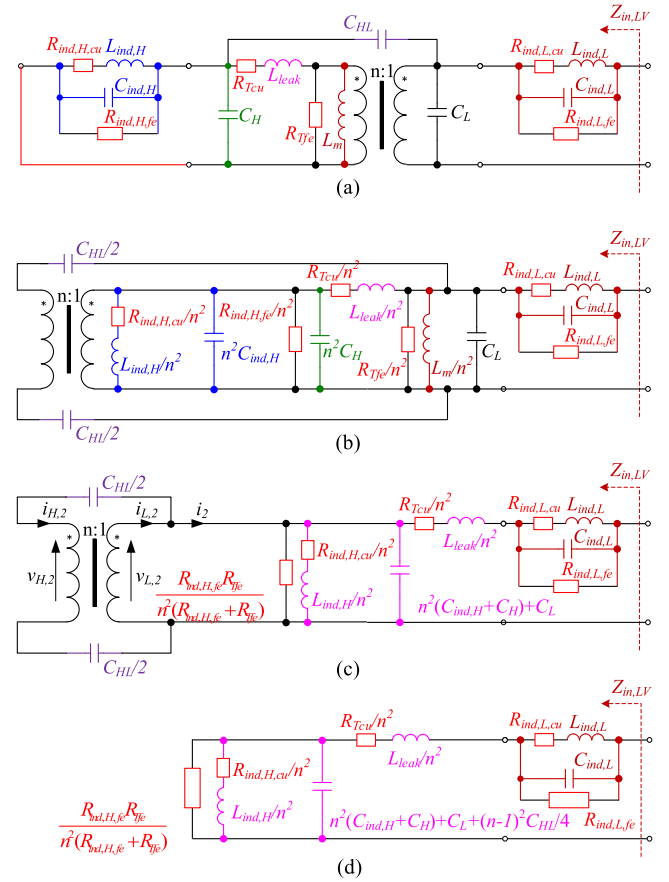


Fig. 6. LV-side input impedance model of the magnetic tank. (a) Detailed model. (b) Intermediate model 1. (c) Intermediate model 2. (d) Simplified model.

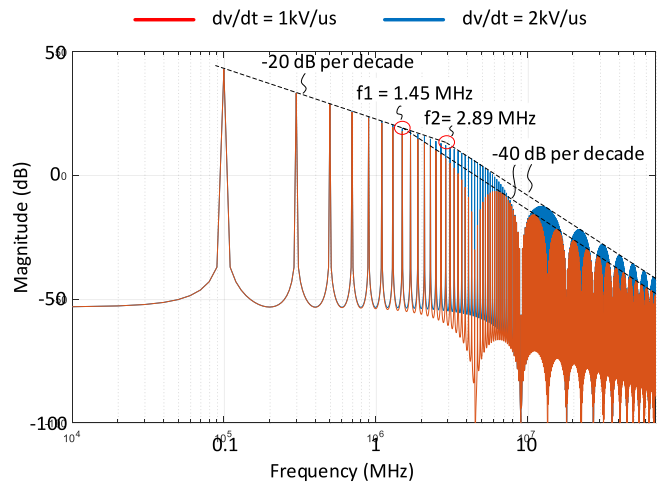


Fig. 7. Spectrum of trapezoidal waveforms @ $f_s = 100\text{ kHz}$ with the same magnitude but different dv/dt .

capacitance is the only parameter needed to be minimized. All the other parasitic capacitances will have marginal influence. The experiments in Section V will verify this.

To summarize and give a clear indication of design concerns regarding the current ringing, a flowchart of the inductor design procedure is shown in Fig. 8. Since several steps are from the

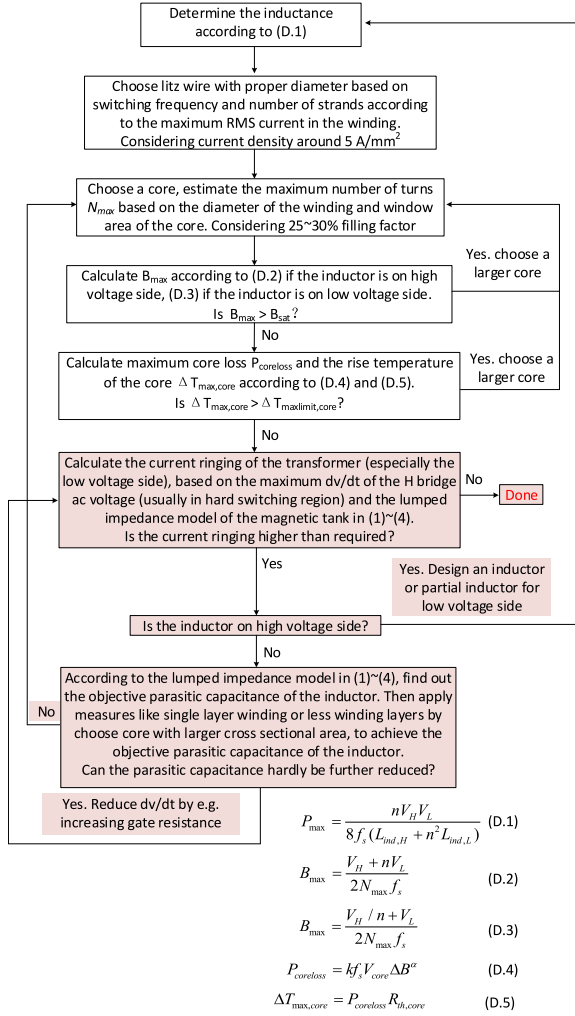


Fig. 8. Flowchart of the inductor design procedure (the concern regarding current ringing is marked in color).

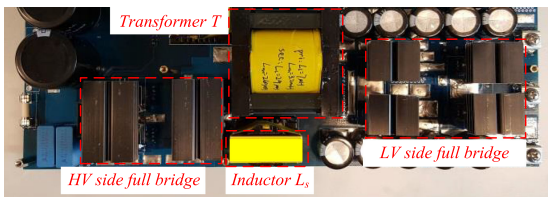


Fig. 9. 2.5-kW DAB converter prototype.

conventional inductor design procedure, only the design steps regarding the current ringing are marked in color.

IV. EXPERIMENTAL VERIFICATION

A 2.5-kW DAB prototype has been built for the validation, as shown in Fig. 9. The switching frequency is 100 kHz, and the nominal HV- and LV-side dc voltages are 400 and 110 V, respectively. The switches used for the HV and LV sides are IPW65R080CFD and IPP110N20N3 (two in parallel), respectively.

The turns ratio of the transformer is $n = 3.5$. The design parameters of the transformer are listed in Table II. By using a

TABLE II
DESIGN PARAMETERS OF THE TRANSFORMER

Parameter	Value
Core type	ETD 59
Core material	Ferrite N97
Primary winding	Litz wire \varnothing 0.2 mm, 90 strands in parallel, 21 turns
Secondary winding	Copper foil 0.15 mm x 35 mm, 2 layers in parallel, 6 turns

TABLE III
DESIGN PARAMETERS OF THE INDUCTORS

Parameter	Value	
	Inductor L_H	Inductor L_L
Core type	ER42V (gapped)	
Core material	Ferrite N87	
Winding	Litz wire \varnothing 0.2 mm	Litz wire \varnothing 0.2 mm
	90 strands in parallel, 17 turns	270 strands in parallel, 5 turns

TABLE IV
MEASURED PARAMETERS OF THE TRANSFORMER AND INDUCTORS

Parameter	Value	Parameter	Value
C_H	77 pF	$L_{ind,H}$	37.5 μ H
C_L	253 pF	$C_{ind,H}$	5.5 pF
C_{HL}	106 pF	$L_{ind,L}$	3.5 μ H
L_{leak}	8 μ H	$C_{ind,L}$	22 pF
L_m	2.5 mH	$R_{ind,H,fe}$	6.5 k Ω
R_{Tje}	8.5 k Ω	$R_{ind,L,fe}$	800 Ω
R_{Tcu}	0.023 Ω	$R_{ind,H,cu}$	0.009 Ω
		$R_{ind,L,cu}$	0.0009 Ω

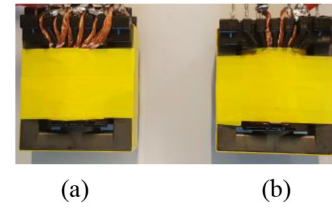


Fig. 10. Picture of the (a) LV- and (b) HV-side inductor.

KEYSIGHT E4990A impedance analyzer, the parameters of the transformer impedance model are obtained, and they are listed in Table IV. The design parameters of the inductors L_{HV} and L_{LV} are listed in Table III. To make a fair comparison between the two inductors, the same type of cores are used, as shown in Fig. 10, and both of their windings are designed as a single layer to minimize the parasitic capacitance [44]. The impedances of the two inductors are measured and shown in Fig. 11(a) and (b). By fitting the curves based on the inductor impedance model in Fig. 3, the model parameters are obtained and they are listed in Table IV. As seen in Fig. 11(a) and (b), the inductor impedance model can match the measured impedance very well. Moreover, compared with the transformer, the winding capacitances of the inductors are much smaller and even their number of turns are

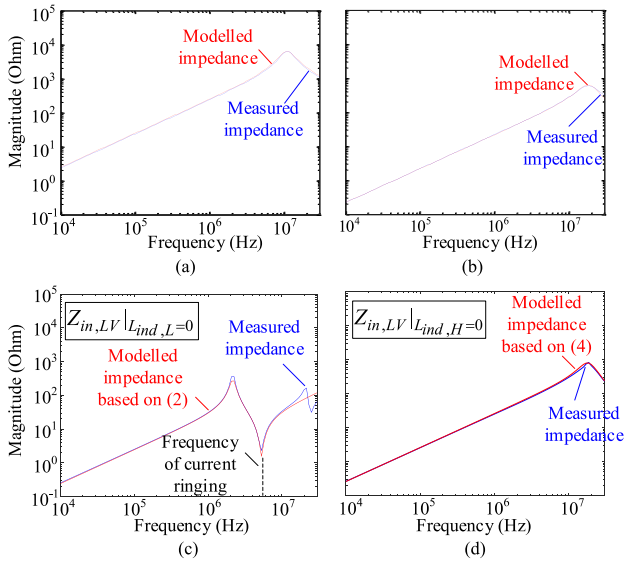


Fig. 11. Comparison between the modeled and measured impedance of (a) HV-side inductor, (b) LV-side inductor. LV-side input impedance of the magnetic tank with (c) only HV-side inductor (d) and only LV-side inductor.

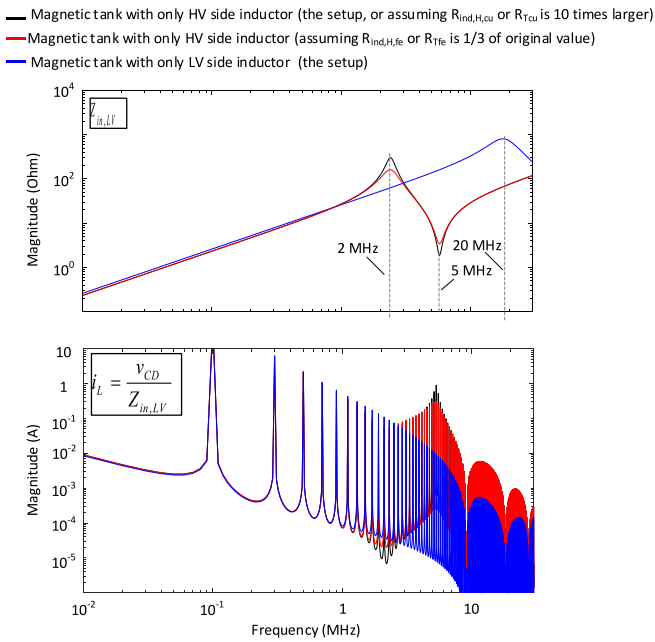


Fig. 12. Impedance of the magnetic tank and LV-side current, influenced by the inductor and the resistance of the magnetic tank.

similar, which proves that the single layer winding structure is effective to reduce the parasitic capacitance. Since the current ringing more often occurs in the LV side winding of the transformer, only the LV-side input impedance $Z_{in, LV}$ of the magnetic tank is tested, as shown in Fig. 11(c) and (d). The fitting curves based on the simplified models of $Z_{in, LV} | L_{ind,L}=0$ and $Z_{in, LV} | L_{ind,H}=0$ in (2) and (4) are also shown. As seen, the simplified models can match the measured impedances very well. $Z_{in, LV} | L_{ind,L}=0$ and $Z_{in, LV} | L_{ind,H}=0$ are then compared in Fig. 12. As seen, they have the same value at a low frequency

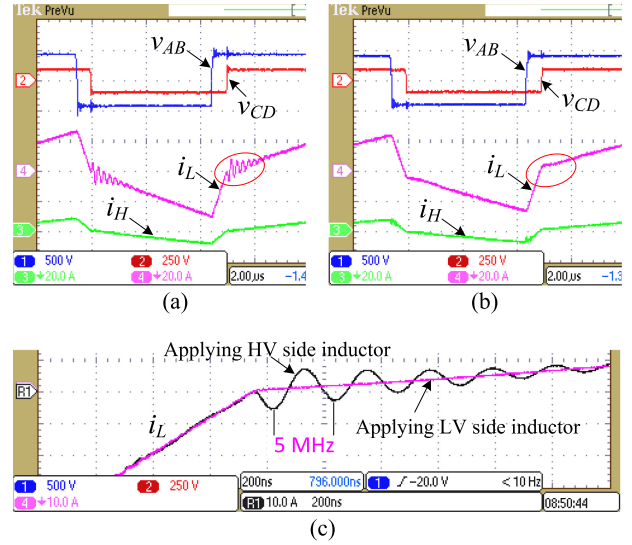


Fig. 13. Experimental results to show the transformer currents with (a) HV-side inductor, (b) LV-side inductor, and (c) zoom in.

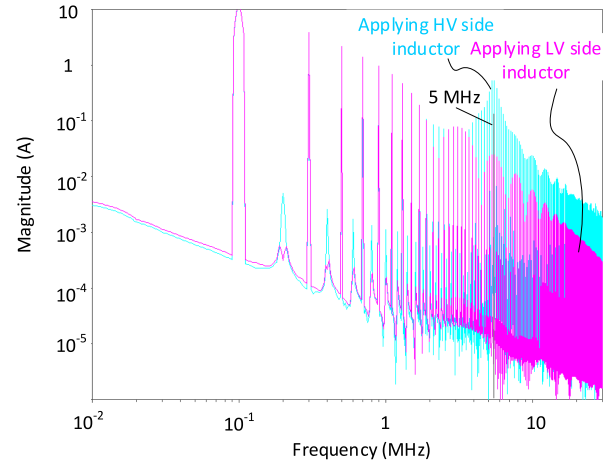


Fig. 14. FFT of i_L obtained in the experimental results.

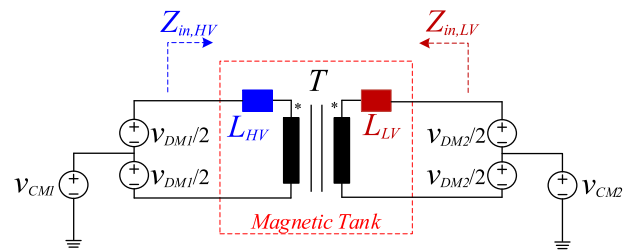


Fig. 15. Equivalent circuit of the DAB converter with the magnetic tank. v_{CM1} and v_{CM2} are the CM voltage sources, and v_{DM1} and v_{DM2} are the differential-mode voltage sources, respectively.

but $Z_{in, LV} | L_{ind,L}=0$ has the first resonant frequency at 2 MHz. Above that, $Z_{in, LV} | L_{ind,L}=0$ becomes capacitive and achieves the valley at 5 MHz. Meanwhile, $Z_{in, LV} | L_{ind,H}=0$ has the first resonant frequency at 20 MHz and the frequency of valley is, of course, higher than that, which reduces the chance of current ringing a lot. The spectrum of $i_L = \frac{v_{CD}}{Z_{in, LV}}$ is then calculated, and it is shown in Fig. 12 as well, where dv/dt of v_{CD} is assumed

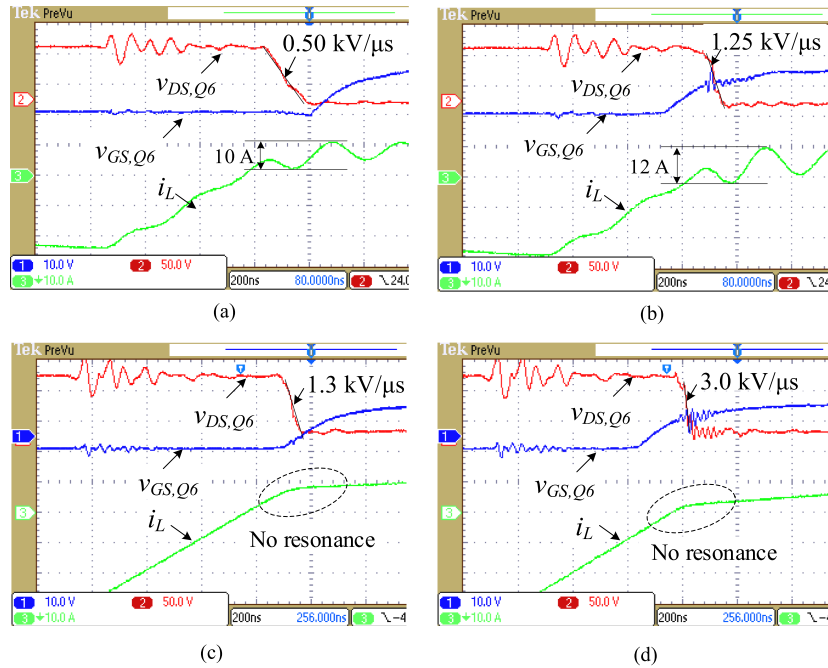


Fig. 16. Experimental results to show the impact of dv/dt and inductor on current ringing, where (a) and (b) have only the HV-side inductor, and (c) and (d) have only the LV-side inductor.

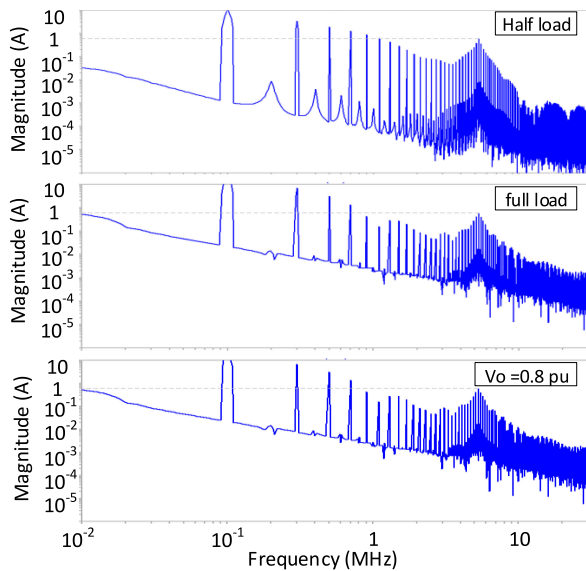


Fig. 17. FFT of i_L when the HV-side inductor is applied ($V_o = 1$ p.u. if not specified).

to be $2 \text{ kV}/\mu\text{s}$. As seen, a peak appears in the spectrum of the i_L with $Z_{in, LV} |_{L_{ind,L}=0}$ at 5 MHz, while it is not the case in the spectrum of the i_L with $Z_{in, LV} |_{L_{ind,H}=0}$. The test results in Fig. 13(c) show that the current ringing happens in i_L at around 5 MHz if the HV-side inductor is used. And there is no current ringing in i_L if the LV-side inductor is used. Moreover, as seen in Fig. 13(a) and (b), i_H has no or much smaller ringing, no matter the HV- or LV-side inductor is used. The fast Fourier transform (FFT) of the i_L in Fig. 13(c) is also obtained and it is shown in Fig. 14. As seen, it matches very well with the calculated FFT in Fig. 12. Besides, the impact of the resistance on the impedance

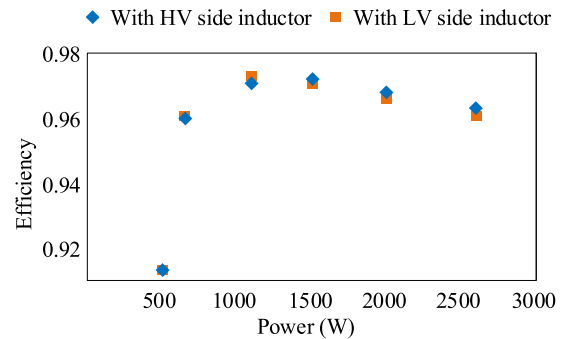


Fig. 18. Overall efficiency of the converter with two different inductor designs.

and current ringing is also indicated in Fig. 12. As seen, the core loss related to the equivalent resistance can significantly influence the peak and valley of the impedance resonance as well as the current ringing. And lower the resistance, lower the current ringing. However, in a proper design, the core loss should be minimized, which means the core loss related resistance cannot be too small. So it is impractical to mitigate the current ringing by reducing the core loss pertaining resistance. The copper loss related resistance does not have visible influence on the impedance curves, even they are ten times larger.

The EMI equivalent circuit of the DAB is derived in [54] and it is combined with the magnetic tank, as shown in Fig. 15. As indicated in Fig. 12, compared with applying the HV-side inductor, applying the LV-side inductor keeps a higher impedance in the differential mode (DM) noises loop from 5 to 30 MHz. Therefore, the DM current in the loop is decreased, as verified in Figs. 12 and 13. For the CM noise, the capacitance of the HV-side inductor is with a higher capacitance (5.5 pF) than the LV-side

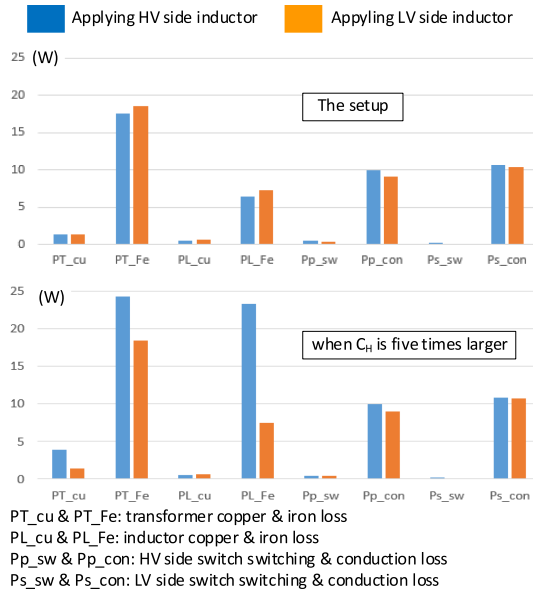


Fig. 19. Loss break down of the converter.

inductor when it is transferred to the HV side (1.8 pF). This is due to the contribution of the larger core-related capacitance and the larger strands of the Litz wire, which induces a larger capacitance. In reality, the HF side inductor will have even larger capacitance due to its high number of turns. So, the multiple layer-winding configuration is usually applied, resulting in significant winding capacitance. Therefore, there is also a smaller CM noise when only using the LV-side inductor.

The impact of dv/dt on the current ringing is also tested and it is shown in Fig. 16. As seen in Fig. 16(a) and (b), when the dv/dt increases from 0.5 kV/ μ s to 1.25 kV/ μ s, the current ringing increases from 10 A to 12 A. But if the HV side inductor is replaced by the LV side inductor [Fig. 16(c) and (d)], the current ringing is gone even the dv/dt increases to 3 kV/ μ s. The current ringing does not change much even the load drops from full load to half, as seen in Fig. 17. When the efficiency difference caused by the inductor design is quite marginal, as seen in Fig. 18, the loss break down is analyzed to show a more concrete comparison in Fig. 19. In the top figure, the loss of most of the components remains the same between the two designs. The transformer copper loss is supposed to be higher when the HV-side inductor is applied. It is due to the current ringing when using the HV-side inductor. The current ringing has a very high frequency, and due to the skin effect, the equivalent ac resistance of the transformer winding is also higher, leading to a higher copper loss. The current ringing is mitigated when applying the LV-side inductor; therefore, the copper loss of the transformer is supposed to be lower. Nonetheless, the current ringing is small, and thereby the loss caused by the current ringing is marginal and has minimal impact on the efficiency. However, if C_H is five times larger, the loss of the transformer and inductor will be significantly influenced, as shown in the bottom figure.

V. CONCLUSION

In this article, the current ringing issues in the DAB converter are thoroughly investigated. The impedance model of the magnetic tank is developed. It showed that the parasitic capacitors in

the magnetic tank affect the current ringing with different weight factors. The position of the inductor and their parasitic capacitors can have a more significant influence on the current ringing than the transformer design. Additionally, the influence of dv/dt is analyzed, which is another factor that can significantly affect the current ringing. In the end, the conventional inductor design procedure is updated with the concern of current ringing.

APPENDIX

A. Modeling of $Z_{in, HV}$

According to Thevenin's theorem, the effect of the LV-side voltage v_{CD} can be eliminated by shorting it. Then by applying the transformer and inductor model in Figs. 2 and 3 into the magnetic tank, an equivalent circuit is obtained, and it is shown in Fig. 5(a). For simplification, the secondary side components are all equivalent to the primary side and the coupling capacitance C_{HL} is split into two, then the circuit in Fig. 5(b) is obtained. L_{leak} is usually much smaller than $L_{ind,H}$, $L_{ind,L}$, and L_m . Moreover $L_m \gg L_{ind,H}$, thus the circuit is further simplified, as shown in Fig. 5(c). According to the definitions of $v_{H,1}$, $v_{L,1}$, and $i_{L,1}$ in Fig. 5(c), they follow

$$\frac{C_{HL}}{2} \frac{d\left(\frac{v_{H,1} - v_{L,1}}{2}\right)}{dt} = -i_{L,1}. \quad (A.1)$$

According to Kirchhoff's current law (KCL), it is obtained

$$i_1 = i_{H,1} - i_{L,1}. \quad (A.2)$$

The voltages and currents of the transformer follow

$$v_{L,1} = v_{H,1}/n \quad (A.3)$$

$$i_{L,1} = ni_{H,1}. \quad (A.4)$$

Substitute (A.2)–(A.4) into (A.1), it is obtained

$$\frac{(1 - 1/n)^2 C_{HL}}{4} \frac{dv_{H,1}}{dt} = i_1. \quad (A.5)$$

According to (A.5), the transformer in Fig. 5(c) together with its coupling capacitance can be equivalent to a capacitor $(1 - 1/n)^2 C_{HL}/4$. Fig. 5(c) is then converted into Fig. 5(d), which is the model of $Z_{in, HV}$.

B. Modeling of $Z_{in, LV}$

Similarly, to model $Z_{in, LV}$, an equivalent circuit of the magnetic tank is obtained and it is shown in Fig. 6(a). The HV-side components will be equal to the LV side and the coupling capacitance is split into two. Then, Fig. 6(b) is obtained. L_{leak}/n^2 is much smaller than $L_{ind,L}$, $\frac{L_{ind,H}}{n^2}$, and L_m/n^2 . Moreover $L_m \gg n^2 L_{ind,L}$, thus Fig. 6(b) is transformed into Fig. 6(c). According to the definitions of $v_{H,2}$, $v_{L,2}$, and $i_{L,2}$ in Fig. 6(c), they follow

$$\frac{C_{HL}}{2} \frac{d\left(\frac{v_{H,2} - v_{L,2}}{2}\right)}{dt} = -i_{H,2}. \quad (A.6)$$

According to KCL, it is obtained

$$i_2 = i_{L,2} - i_{H,2}. \quad (A.7)$$

The voltages and currents of the transformer follow

$$v_{L,2} = v_{H,2}/n \quad (\text{A.8})$$

$$i_{L,2} = ni_{H,2}. \quad (\text{A.9})$$

Substitute (A.7)–(A.9) into (A.6), it is obtained

$$\frac{(n-1)^2 C_{HL}}{4} \frac{dv_{L,2}}{dt} = -i_2. \quad (\text{A.10})$$

According to (A.10), the transformer in Fig. 6(c) together with its coupling capacitance can be equivalent to a capacitor $(n-1)^2 C_{HL}/4$. Fig. 6(c) is then converted into Fig. 6(d), which is the model of $Z_{in, LV}$.

REFERENCES

- [1] R. W. D. Doncker, D. M. Divan, and M. H. Kheraluwala, "A three-phase soft-switched high power density DC/DC converter for high-power applications," in *Proc. Conf. Rec. IEEE Ind. Appl. Soc. Annu. Meeting*, Oct. 1988, vol. 1, pp. 796–805.
- [2] M. Liserre, G. Buticchi, M. Andresen, G. D. Carne, L. F. Costa, and Z.-X. Zou, "The smart transformer: Impact on the electric grid and technology challenges," *IEEE Ind. Electron. Mag.*, vol. 10, no. 2, pp. 46–58, Jun. 2016.
- [3] J. Ge, Z. Zhao, L. Yuan, and T. Lu, "Energy feed-forward and direct feed-forward control for solid-state transformer," *IEEE Trans. Power Electron.*, vol. 30, no. 8, pp. 4042–4047, Aug. 2015.
- [4] B. Zhao, Q. Song, W. Liu, and Y. Sun, "Overview of dual-active-bridge isolated bidirectional DC–DC converter for high-frequency-link power-conversion system," *IEEE Trans. Power Electron.*, vol. 29, no. 8, pp. 4091–4106, Aug. 2014.
- [5] L. Xue, Z. Shen, D. Boroyevich, P. Mattavelli, and D. Diaz, "Dual active bridge-based battery charger for plug-in hybrid electric vehicle with charging current containing low frequency ripple," *IEEE Trans. Power Electron.*, vol. 30, no. 12, pp. 7299–7307, Dec. 2015.
- [6] S. Anwar, W. Zhang, F. Wang, and D. J. Costinett, "Integrated dc-dc converter design for electric vehicle powertrains," in *Proc. IEEE Appl. Power Electron. Conf. Expo.*, 2016, pp. 424–431.
- [7] S. P. Engel, M. Stieneker, N. Soltau, S. Rabiee, H. Stagge, and R. W. D. Doncker, "Comparison of the modular multilevel dc converter and the dual-active bridge converter for power conversion in HVDC and MVDC grids," *IEEE Trans. Power Electron.*, vol. 30, no. 1, pp. 124–137, Jan. 2015.
- [8] P. Purgat, R. A. Prakoso, L. Mackay, Z. Qin, L. Ramirez-Elizondo, and P. Bauer, "A partially rated DC-DC converter for power flow control in meshed LVDC distribution grids," in *Proc. IEEE Appl. Power Electron. Conf. Expo.*, 2018, pp. 1591–1596.
- [9] P. Purgat, N. H. van der Blij, Z. Qin, and P. Bauer, "Partially rated power flow control converter modeling for low-voltage DC grids," *IEEE J. Emerg. Sel. Topics Power Electron.*, vol. 8, no. 3, pp. 2430–2444, Sep. 2020.
- [10] J. Everts, F. Krismer, J. V. den Keybus, J. Driesen, and J. W. Kolar, "Optimal ZVS modulation of single-phase single-stage bidirectional DAB AC–DC converters," *IEEE Trans. Power Electron.*, vol. 29, no. 8, pp. 3954–3970, Aug. 2014.
- [11] T. Todorčević, R. van Kessel, P. Bauer, and J. A. Ferreira, "A modulation strategy for wide voltage output in DAB-based DC–DC modular multilevel converter for DEAP wave energy conversion," *IEEE J. Emerg. Sel. Topics Power Electron.*, vol. 3, no. 4, pp. 1171–1181, Dec. 2015.
- [12] Z. Qin, Y. Shen, P. C. Loh, H. Wang, and F. Blaabjerg, "A dual active bridge converter with an extended high-efficiency range by DC blocking capacitor voltage control," *IEEE Trans. Power Electron.*, vol. 33, no. 7, pp. 5949–5966, Jul. 2018.
- [13] B. Cui, P. Xue, and X. Jiang, "Elimination of high frequency oscillation in dual active bridge converters by dv/dt optimization," *IEEE Access*, vol. 7, pp. 55554–55564, 2019.
- [14] R. T. Naayagi, "Electromagnetic compatibility issues of dual active bridge DC-DC converter," in *Proc. Int. Conf. Energy Efficient Technol. Sustain.*, 2013, pp. 699–703.
- [15] Z. Shen, H. Wang, Y. Shen, Z. Qin, and F. Blaabjerg, "An improved stray capacitance model for inductors," *IEEE Trans. Power Electron.*, vol. 34, no. 11, pp. 11153–11170, Nov. 2019.
- [16] J. Biela and J. W. Kolar, "Using transformer parasitics for resonant converters—A review of the calculation of the stray capacitance of transformers," *IEEE Trans. Ind. Appl.*, vol. 44, no. 1, pp. 223–233, Jan./Feb. 2008.
- [17] P. Thummala, H. Schneider, Z. Zhang, and M. A. E. Andersen, "Investigation of transformer winding architectures for high-voltage (2.5 kV) capacitor charging and discharging applications," *IEEE Trans. Power Electron.*, vol. 31, no. 8, pp. 5786–5796, Aug. 2016.
- [18] B. Liu, R. Ren, F. Wang, D. Costinett, and Z. Zhang, "Winding scheme with fractional layer for differential-mode toroidal inductor," *IEEE Trans. Ind. Electron.*, vol. 67, no. 2, pp. 1592–1604, Feb. 2020.
- [19] X. Liu, Y. Wang, J. Zhu, Y. Guo, G. Lei, and C. Liu, "Calculation of capacitance in high-frequency transformer windings," *IEEE Trans. Magn.*, vol. 52, no. 7, Jul. 2016, Art. no. 2003204.
- [20] M. S. S. Nia, P. Shamsi, and M. Ferdowsi, "Investigation of various transformer topologies for HF isolation applications," *IEEE Trans. Plasma Sci.*, vol. 48, no. 2, pp. 512–521, Feb. 2020.
- [21] R. Chattopadhyay, M. A. Juds, P. R. Ohodnicki, and S. Bhattacharya, "Modelling, design and analysis of three limb high frequency transformer including transformer parasitics, for SiC mosfet based three port DAB," in *Proc. 42nd Annu. Conf. IEEE Ind. Electron. Soc.*, Florence, Italy, 2016, pp. 4181–4186.
- [22] L. F. de Freitas Gutierrez and G. Cardoso, "Analytical technique for evaluating stray capacitances in multiconductor systems: Single layer air-core inductors," *IEEE Trans. Power Electron.*, vol. 33, no. 7, pp. 6147–6158, Jul. 2018.
- [23] M. Aghaei and S. Kaboli, "On the effect of disorder on stray capacitance of transformer winding in high-voltage power supplies," *IEEE Trans. Ind. Electron.*, vol. 64, no. 5, pp. 3608–3618, May 2017.
- [24] Z. Shen and H. Wang, "Parasitics of orthocyclic windings in inductors and transformers," *IEEE Trans. Power Electron.*, vol. 36, no. 2, pp. 1994–2008, Feb. 2021.
- [25] Z. Ouyang, O. C. Thomsen, and M. A. E. Andersen, "Optimal design and tradeoff analysis of planar transformer in high power dc-dc converters," *IEEE Trans. Ind. Electron.*, vol. 59, no. 7, pp. 2800–2810, Jul. 2012.
- [26] M. A. Saket, N. Shafiei, and M. Ordóñez, "LLC converters with planar transformers: Issues and mitigation," *IEEE Trans. Power Electron.*, vol. 32, no. 6, pp. 4524–4542, Jun. 2017.
- [27] L. A. R. Tria, D. Zhang, and J. E. Fletcher, "High-frequency planar transformer parameter estimation," *IEEE Trans. Magn.*, vol. 51, no. 11, Nov. 2015, Art. no. 8402604.
- [28] P. L. Dowell, "Effects of eddy currents in transformer windings," *Proc. Inst. Elect. Eng.*, vol. 113, no. 8, pp. 1387–1394, Aug. 1966.
- [29] D. Whitman and M. K. Kazimierzczuk, "An analytical correction to Dowell's equation for inductor and transformer winding losses using cylindrical coordinates," *IEEE Trans. Power Electron.*, vol. 34, no. 11, pp. 10425–10432, Nov. 2019.
- [30] M. A. Bahmani, T. Thiringer, and H. Ortega, "An accurate pseudoempirical model of winding loss calculation in HF foil and round conductors in switchmode magnetics," *IEEE Trans. Power Electron.*, vol. 29, no. 8, pp. 4231–4246, Aug. 2014.
- [31] C. Feeny, J. Zhang, and M. Duffy, "AC winding loss of phase shifted coupled windings," *IEEE Trans. Power Electron.*, vol. 31, no. 2, pp. 1472–1478, Feb. 2016.
- [32] B. A. Reese and C. R. Sullivan, "Litz wire in the MHz range: Modeling and improved designs," in *Proc. IEEE 18th Workshop Control Model. Power Electron.*, Stanford, CA, USA, 2017, pp. 1–8.
- [33] E. L. Barrios, A. Ursua, L. Marroyo, and P. Sanchis, "Analytical design methodology for Litz-wired high-frequency power transformers," *IEEE Trans. Ind. Electron.*, vol. 62, no. 4, pp. 2103–2113, Apr. 2015.
- [34] R. P. Wojda and M. K. Kazimierzczuk, "Winding resistance and power loss of inductors with Litz and solid-round wires," *IEEE Trans. Ind. Appl.*, vol. 54, no. 4, pp. 3548–3557, Jul./Aug. 2018.
- [35] Z. Ouyang, J. Zhang, and W. G. Hurley, "Calculation of leakage inductance for high-frequency transformers," *IEEE Trans. Power Electron.*, vol. 30, no. 10, pp. 5769–5775, Oct. 2015.
- [36] M. A. Bahmani and T. Thiringer, "Accurate evaluation of leakage inductance in high-frequency transformers using an improved frequency dependent expression," *IEEE Trans. Power Electron.*, vol. 30, no. 10, pp. 5738–5745, Oct. 2015.
- [37] A. Fouineau, M.-A. Raulet, B. Lefebvre, N. Burais, and F. Sixdenier, "Semi-analytical methods for calculation of leakage inductance and frequency-dependent resistance of windings in transformers," *IEEE Trans. Magn.*, vol. 54, no. 10, Oct. 2018, Art. no. 8400510.
- [38] K. Zhang *et al.*, "Accurate calculation and sensitivity analysis of leakage inductance of high-frequency transformer with litz wire winding," *IEEE Trans. Power Electron.*, vol. 35, no. 4, pp. 3951–3962, Apr. 2020.
- [39] F. Pan, L. Jin, P. Pan, and Z. Xu, "Design procedure of the leakage inductance for a pulse transformer considering winding structures," *IEEE Trans. Plasma Sci.*, vol. 45, no. 9, pp. 2504–2510, Sep. 2017.

- [40] M. Nazmunahar, S. Simizu, P. R. Ohodnicki, S. Bhattacharya, and M. E. McHenry, "Finite-element analysis modeling of high-frequency single-phase transformers enabled by metal amorphous nanocomposites and calculation of leakage inductance for different winding topologies," *IEEE Trans. Magn.*, vol. 55, no. 7, Jul. 2019, Art. no. 8401511.
- [41] R. Chattopadhyay, M. A. Juds, G. Gohil, S. Gulur, P. R. Ohodnicki, and S. Bhattacharya, "Optimized design for three port transformer considering leakage inductance and parasitic capacitance," in *Proc. IEEE Energy Convers. Congr. Expo.*, Cincinnati, OH, USA, 2017, pp. 3247–3254.
- [42] Z. Ouyang, W. G. Hurley, and M. A. E. Andersen, "Improved analysis and modeling of leakage inductance for planar transformers," *IEEE Trans. Emerg. Sel. Topics Power Electron.*, vol. 7, no. 4, pp. 2225–2231, Dec. 2019.
- [43] M. Zdanowski, J. Rabkowski, K. Kostov, R. Barlik, and H.-P. Nee, "Design and evaluation of reduced self-capacitance inductor in DC/DC converters with fast-switching SiC transistors," *IEEE Trans. Power Electron.*, vol. 29, no. 5, pp. 2492–2499, May 2014.
- [44] J. C. Hernandez, L. P. Petersen, and M. A. E. Andersen, "Low capacitive inductors for fast switching devices in active power factor correction applications," in *Proc. Int. Power Electron. Conf.*, Hiroshima, Japan, 2014, pp. 3352–3357.
- [45] M. Pahlevaninezhad, D. Hamza, and P. K. Jain, "An improved layout strategy for common-mode EMI suppression applicable to high-frequency planar transformers in high-power DC/DC converters used for electric vehicles," *IEEE Trans. Power Electron.*, vol. 29, no. 3, pp. 1211–1228, Mar. 2014.
- [46] M. A. Saket, M. Ordóñez, and N. Shafiei, "Planar transformers with near-zero common-mode noise for flyback and forward converters," *IEEE Trans. Power Electron.*, vol. 33, no. 2, pp. 1554–1571, Feb. 2018.
- [47] Y. Li, H. Zhang, S. Wang, H. Sheng, C. P. Chng, and S. Lakshminathan, "Investigating switching transformers for common mode EMI reduction to remove common mode EMI filters and y-capacitors in flyback converters," *IEEE Trans. Emerg. Sel. Topics Power Electron.*, vol. 6, no. 4, pp. 2287–2301, Dec. 2018.
- [48] Z. Shen *et al.*, "The faraday shields loss of transformers," *IEEE Trans. Power Electron.*, vol. 35, no. 11, pp. 12194–12206, Nov. 2020.
- [49] Z. Yang, J. Hu, G. C. Pasupuleti, and R. W. D. Doncker, "Operation-oriented design procedure of a three-phase dual-active bridge converter for a wide operation range," in *Proc. IEEE Energy Convers. Congr. Expo.*, Portland, OR, USA, 2018, pp. 2835–2842.
- [50] M. Noah, T. Shirakawa, K. Umetani, J. Imaoka, M. Yamamoto, and E. Hiraki, "Effects of secondary leakage inductance on the LLC resonant converter," *IEEE Trans. Power Electron.*, vol. 35, no. 1, pp. 835–852, Jan. 2020.
- [51] J. Riedel, D. G. Holmes, B. P. McGrath, and C. Teixeira, "Active suppression of selected DC bus harmonics for dual active bridge DC–DC converters," *IEEE Trans. Power Electron.*, vol. 32, no. 11, pp. 8857–8867, Nov. 2017.
- [52] Z. Qin, Z. Shen, F. Blaabjerg, and P. Bauer, "Modelling, analysis and mitigation of the transformer current ringing in dual active bridge converters," in *Proc. IEEE Energy Convers. Congr. Expo.*, Portland, OR, USA, 2018, pp. 650–655.
- [53] Module 3: Signals and Spectra, Aug. 28, 2020. [Online]. Available: https://www.egr.msu.edu/emrg/sites/default/files/content/module3_signals_and_spectra.pdf
- [54] G. Buticchi, D. Barater, L. F. Costa, and M. Liserre, "A PV-inspired low-common-mode dual-active-bridge converter for aerospace applications," *IEEE Trans. Power Electron.*, vol. 33, no. 12, pp. 10467–10477, Dec. 2018.



Zian Qin (Senior Member, IEEE) received the B.Eng. degree in automation from Beihang University, Beijing, China, in 2009, the M.Eng. degree in control science and engineering from the Beijing Institute of Technology, Beijing, in 2012, and the Ph.D. degree in electrical engineering from Aalborg University, Aalborg, Denmark, in 2015.

In 2014, he was a Visiting Scientist with RWTH Aachen University, Aachen, Germany. From 2015 to 2017, he was a Postdoctoral Research Fellow with Aalborg University. He is currently an Assistant Professor with the Delft University of Technology, Delft, Netherlands. He serves as the Technical Program Chair of IEEE-ISIE 2020, Technical Program Cochair of IEEE-COMPEL 2020, and Industrial Session Cochair of ECCE-Asia 2020. His research interests include wide bandgap devices, power electronics-based grid, and Power2X.



Zhan Shen (Member, IEEE) received the B.E. degree in electrical engineering and automation from the Nanjing University of Aeronautics and Astronautics, Nanjing, China, in 2013, the M.E. degree in electrical engineering from Southeast University, Nanjing, in 2016, the master's thesis with RWTH Aachen University, Aachen, Germany, in February 2016, and the Ph.D. degree in power electronics from the Center of Reliable Power Electronics, Aalborg University, Aalborg, Denmark, in 2020.

From October 2018 to January 2019, he was a Visiting Scholar with the Massachusetts Institute of Technology, Cambridge, MA, USA, and a Visiting Student. He was with the ABB Corporate Research Center, Beijing, China, in 2016. He is currently a Postdoctoral Research Fellow with Aalborg University, Aalborg. His research interests include modeling, design, and life-cycle performance optimization of magnetic components and EMI filters in power electronics.



Frede Blaabjerg (Fellow, IEEE) received the Ph.D. degree in electrical engineering from Aalborg University, Aalborg, Germany, in 1995.

From 1987 to 1988, he was with ABB-Scandia, Randers, Denmark. From 1988 to 1992, he became an Assistant Professor in 1992, an Associate Professor in 1996, and a Full Professor of power electronics and drives in 1998. In 2017, he became a Villum Investigator. He is an honoris causa at University Politehnica Timisoara, Timisoara, Romania, and

Tallinn Technical University, Tallinn, Estonia. He is the coauthor of four monographs and editor of ten books in power electronics and its applications. He is nominated in 2014–2019 by Thomson Reuters to be between the most 250 cited researchers in engineering in the world. His current research interests include power electronics and its applications, such as in wind turbines, PV systems, reliability, harmonics, and adjustable speed drives. He has authored or coauthored more than 600 journal papers in the fields of power electronics and its applications.

Dr. Blaabjerg was a recipient of 32 IEEE Prize Paper Awards, the IEEE PELS Distinguished Service Award in 2009, the EPE-PEMC Council Award in 2010, the IEEE William E. Newell Power Electronics Award 2014, the Villum Kann Rasmussen Research Award 2014, the Global Energy Prize in 2019, and the 2020 IEEE Edison Medal. He was the Editor-in-Chief of the IEEE TRANSACTIONS ON POWER ELECTRONICS from 2006 to 2012. He has been a Distinguished Lecturer for the IEEE Power Electronics Society from 2005 to 2007 and for the IEEE Industry Applications Society from 2010 to 2011 as well as 2017 to 2018. Since 2019, he has been serving as the President of the IEEE Power Electronics Society. He is also the Vice-President of the Danish Academy of Technical Sciences.



Pavol Bauer (Senior Member, IEEE) received the master's degree from the Technical University of Kosice, Košice, Slovakia, in 1985, and the Ph.D. degree from the Delft University of Technology, Delft, Netherlands, in 1995, both in electrical engineering.

He received the title prof. from the President of the Czech Republic at the Brno University of Technology, Brno, Czech Republic, in 2008, and Delft University of Technology, Delft, in 2016. He is currently a Full Professor with the Department

of Electrical Sustainable Energy, Delft University of Technology, Delft, and the Head of DC Systems, Energy Conversion, and Storage Group. He has authored or coauthored more than 72 journals and almost 300 conference papers in my field (with H factor Google scholar 43, Web of science 20), is an author or coauthor of eight books, holds four international patents, and organized several tutorials at the international conferences. He has worked on many projects for industry concerning wind and wave energy, power electronic applications for power systems, such as Smarttrafo, HVdc systems, projects for smart cities, such as PV charging of electric vehicles, PV and storage integration, and contactless charging. He participated in several Leonardo da Vinci and H2020 EU projects as a Project Partner (ELINA, INETELLE, and E-Pragmatic) and Coordinator (PEMCWebLab.com-Edipe, SustEner, and Eranet DCMICRO).